HAL
open science

Non-targeted 13 C metabolite analysis demonstrates broad re-orchestration of leaf metabolism when gas exchange conditions vary

Cyril Abadie, Julie Lalande, Anis Limami, Guillaume Tcherkez

To cite this version:

Cyril Abadie, Julie Lalande, Anis Limami, Guillaume Tcherkez. Non-targeted 13 C metabolite analysis demonstrates broad re-orchestration of leaf metabolism when gas exchange conditions vary. Plant, Cell and Environment, 2020, 44 (2), pp.445-457. 10.1111/pce.13940 . hal-03033342

HAL Id: hal-03033342

https://hal.inrae.fr/hal-03033342v1

Submitted on 1 Dec 2020

HAL is a multi-disciplinary open access archive for the deposit and dissemination of scientific research documents, whether they are published or not. The documents may come from teaching and research institutions in France or abroad, or from public or private research centers.

L'archive ouverte pluridisciplinaire **HAL**, est destinée au dépôt et à la diffusion de documents scientifiques de niveau recherche, publiés ou non, émanant des établissements d'enseignement et de recherche français ou étrangers, des laboratoires publics ou privés.

Received: 12 September 2020 | Revised: 2 November 2020 | Accepted: 3 November 2020
DOI: 10.1111/pce.13940

ORIGINAL ARTICLE

Plant, Cell & Environment WILEY

Non-targeted ^{13}C metabolite analysis demonstrates broad re-orchestration of leaf metabolism when gas exchange conditions vary

Cyril Abadie[1] | Julie Lalande[1] | Anis M. Limami[1] | Guillaume Tcherkez[1,2]

[1]Institut de Recherche en Horticulture et Semences, INRA d'Angers, Université d'Angers, Angers, France

[2]Research School of Biology, ANU Joint College of Sciences, Australian National University, Canberra, Australia

Correspondence
Guillaume Tcherkez, Institut de Recherche en Horticulture et Semences, INRA d'Angers, Université d'Angers, 42 rue Georges Morel, 49070 Beaucouzé, Angers, France.
Email: guillaume.tcherkez@anu.edu.au

Funding information
Conseil Régional des Pays de la Loire, Grant/Award Number: Connect Talent Isoseed

Abstract

It is common practice to manipulate CO_2 and O_2 mole fraction during gas-exchange experiments to suppress or exacerbate photorespiration, or simply carry out CO_2 response curves. In doing so, it is implicitly assumed that metabolic pathways other than carboxylation and oxygenation are altered minimally. In the past few years, targeted metabolic analyses have shown that this assumption is incorrect, with changes in the tricarboxylic acid cycle, anaplerosis (phospho*enol*pyruvate carboxylation), and nitrogen or sulphur assimilation. However, this problem has never been tackled systematically using non-targeted analyses to embrace all possible affected metabolic pathways. Here, we exploited combined NMR, GC–MS, and LC–MS data and conducted non-targeted analyses on sunflower leaves sampled at different O_2/CO_2 ratios in a gas exchange system. The statistical analysis of nearly 4,500 metabolic features not only confirms previous findings on anaplerosis or S assimilation, but also reveals significant changes in branched chain amino acids, phenylpropanoid metabolism, or adenosine turn-over. Noteworthy, all of these pathways involve CO_2 assimilation or liberation and thus affect net CO_2 exchange. We conclude that manipulating CO_2 and O_2 mole fraction has a broad effect on metabolism, and this must be taken into account to better understand variations in carboxylation (anaplerotic fixation) or apparent day respiration.

KEYWORDS
day respiration, gas-exchange, isotopic labelling, metabolomics, photorespiration, photosynthesis

1 | INTRODUCTION

Net CO_2 assimilation is the result of carboxylation (v_c), CO_2 release by photorespiration (v_o/ξ, where v_o is the oxygenation rate and ξ is a stoichiometric coefficient, very close to 2 [Abadie, Boex-Fontvieille, Carroll, & Tcherkez, 2016; Busch, 2020]) and CO_2 production by day respiration (R_d). In gas-exchange experiments, the balance between carboxylation and oxygenation is routinely manipulated using CO_2 and O_2 mole fraction, for example using high CO_2 or low O_2 (0.5 or 2%) to suppress photorespiration. In fact, the oxygenation-to-carboxylation ratio, v_o/v_c, linearly depends on the concentration ratio of dissolved gases at carboxylation sites, $[O_2]/[CO_2]$. It is commonly assumed that the impact of changing $[O_2]/[CO_2]$ on other pathways and in particular on R_d is negligible (von Caemmerer, 2013).

However, in the past few years, strong evidence has been provided that in the short term, CO_2 and O_2 mole fraction changes the flux through several metabolic pathways. In particular, at high photorespiration (low CO_2 or high O_2 condition), there is an increase in anaplerotic CO_2 fixation by phospho*enol*pyruvate carboxylase (PEPC) (Abadie & Tcherkez, 2019a). When photosynthesis is low, this

 © 2020 John Wiley & Sons Ltd

represents a substantial CO_2 fixation flux, of up to 40% of total observed assimilation. In addition, high photorespiration is associated with enhanced activity of the tricarboxylic acid pathway, probably leading to an increase day respiratory rate R_d (Griffin & Turnbull, 2013; Tcherkez et al., 2008, 2012). It must be noted that in the previous sentence, the term "probably" has been used. In effect, the measurement of R_d is still technically challenging and the two common methods (Kok and Laisk methods) used to determine R_d have drawbacks (Atkin, Millar, Gardeström, & Day, 2000; Tcherkez et al., 2017): the Kok effect has recently been shown to involve specific metabolism and numerically, cannot simply be explained by a change in CO_2 evolution (Gauthier, Saenz, Griffin, Way, & Tcherkez, 2020), meaning that Kok-derived estimates of R_d are not fully representative; the Laisk method requires changes in CO_2 mole fraction, thus it is not adapted to examine the effect of the gaseous environment. Conversely, at low O_2 (2% O_2 and below), leaves experience hypoxic metabolism leading to alanine accumulation, diverting pyruvate from mitochondrial oxidation thereby impacting on day respiration (Abadie, Blanchet, Carroll, & Tcherkez, 2017). Using the Kok method, it has been suggested that under 2% O_2, R_d is ≈20% lower than at 21% O_2 (Tcherkez, Mahe, et al., 2012).

In addition to changes in day respiration or PEPC activity, changing O_2/CO_2 conditions has been shown to alter the balance between sugar species (sucrose, glucose and fructose) (Abadie, Bathellier, & Tcherkez, 2018) and modifies the flux associated with N and S assimilation. In effect, high photorespiration stimulates N assimilation (Bloom, Burger, Asensio, & Cousins, 2010; Bloom, Burger, Kimball, & Pinter, 2014; Rachmilevitch, Cousins, & Bloom, 2004), probably because of the transient higher need in glutamate for glycine synthesis and accumulation when O_2/CO_2 increases. High photorespiration also stimulates sulphate reduction and S assimilation to methionine, partly because of the higher turn-over in C_1 units carried by tetrahydrofolate (THF) and the higher availability in serine (Abadie & Tcherkez, 2019b). However, protein synthesis increases with net photosynthesis (and thus when the CO_2 mole fraction increases and O_2 mole fraction decreases, except under hypoxia) via the stimulation of cytoplasmic translation initiation and this effect is most likely signalled by sugars rather than amino acid availability (Tcherkez et al., 2020).

Taken as a whole, O_2/CO_2 conditions affect not only primary products of photosynthesis and photorespiration, but also other metabolites, with potential impacts on apparent carboxylation and apparent day respiration. The overall effect of presumably most important non-photosynthetic and non-photorespiratory pathways during gas-exchange has been reviewed recently (Tcherkez & Limami, 2019). However, our current knowledge comes from targeted analyses on pathways that are anticipated to be most impacted by the carboxylation-to-oxygenation ratio. In other words, there is presently no systematic, non-targeted analysis of changes triggered by O_2/CO_2 conditions during gas-exchange. This lack of knowledge is problematic, in particular to understand the metabolic significance of variables of net photosynthesis such as R_d. In effect, R_d represents the non-photorespiratory CO_2 evolution rate in the light and is ordinarily assumed to reflect decarboxylation by classical metabolic pathways: pyruvate dehydrogenation (by mitochondrial and chloroplastic pyruvate dehydrogenase complexes), cytosolic oxidative pentose phosphate pathway (and perhaps also in the chloroplast, [Preiser, Fisher, Banerjee, & Sharkey, 2019]) and the tricarboxylic acid pathway (Tcherkez, Boex-Fontvieille, Mahé, & Hodges, 2012). Having said that, minor pathways such as de novo amino acid synthesis could be accompanied by CO_2 release or require aspartate as a building block and thus CO_2 fixation by PEPC, and the flux in such pathways can vary with O_2/CO_2.

As an aid in clarifying this aspect, we exploited labelling and metabolomics data and used full datasets to conduct a non-targeted analysis. Sunflower (*Helianthus annuus* L.) leaves were placed in a gas-exchange system under different O_2/CO_2 conditions (with $^{13}CO_2$) and when in the photosynthetic steady state, were instant-frozen with liquid nitrogen spraying. Analyses were carried out by nuclear magnetic resonance, gas chromatography coupled to nominal mass spectrometry, and liquid chromatography coupled to exact mass spectrometry on the same samples. Sunflower was used as a model species here because it contains detectable levels of secondary metabolites (phenylpropanoids) and amino acid derivatives (such as metabolites of the leucine-isoleucine pathway), making the examination of multiple pathways relatively easy. In addition, leaves are sufficiently large to generate big samples and thus allow NMR analyses. The use of ^{13}C-labelling allowed us to identify metabolite isotopologues that were turned-over using carbon coming from current photosynthesis. The statistical analysis (both univariate and multivariate) of O_2/CO_2 conditions was conducted on the different isotopologues taken separately, so as to differentiate effects on pool size and turn-over. Our results show that in addition to the above-cited effects (such as PEPC activity or S assimilation), O_2/CO_2 conditions impact on phenylpropanoids, branched chain and aspartate-derived amino acids, and adenosine turn-over.

2 | MATERIAL AND METHODS

2.1 | Plant material

Sunflower seeds (*Helianthus annuus*, var. XRQ) were directly sown in potting mix and transferred to 15 L pots after 2 weeks (filled with Martins potting mix). Plants were grown in the greenhouse under 24/18°C, 60/55% relative humidity, 16/8 h photoperiod (day/night), with natural light supplemented by Lucagrow 400 W sodium lamps (JB Lighting, Cheltenham, Australia). Plants were watered every 2 days supplemented once a week with 1.5 g/L nutrient solution Peters Professional Pot Plant Special (Everris, Netherlands) with an $N/P_2O_5/K_2O$ composition of 15/11/29 (and a nitrogen balance nitrate/ammonium/urea of 8.6/2.0/4.4). Plants were used for experiments 50 days after sowing. We used leaves of rank 5 to 7, which are the mature source leaves with maximum photosynthetic capacity at this developmental stage.

2.2 | Gas exchange and sampling

The overall design of the experiment is depicted in Figure S1. Plants used for gas-exchange and labelling were taken from the glasshouse at fixed time (4 hr after the onset of light) so as to avoid potential diel cycle effects. Gas-exchange under controlled O_2/CO_2 conditions and sampling was done as in (Abadie & Tcherkez, 2019a). Briefly, an adapted chamber was coupled to the LI-COR 6400-XT (LI-COR Biosciences, USA) and had soft transparent walls to allow instant sampling by liquid nitrogen spraying. Gas-exchange conditions were: 400 μmol m^{-2} s^{-1} photosynthetically active radiation (PAR), 80% relative humidity, gas flow 35 L/h, and 21–23°C air temperature. Isotopic labelling was performed using $^{13}CO_2$ (Sigma-Aldrich, 99% ^{13}C) for 2 hr after 1 hr of photosynthetic induction to reach the photosynthetic steady state. This time window (2 hr labelling) has been selected here to both allow sufficient labelling and avoid too high ^{13}C-signal overlapping in NMR spectra (Abadie et al., 2018). For all O_2/CO_2 conditions, two series of experiments were done: with $^{13}CO_2$, and with natural CO_2. The six O_2/CO_2 conditions presented here are (%/μmol/mol, ordered by increasing carboxylation-to-oxygenation ratio): 100/380, 21/140, 21/380, 21/800, 2/380 and 0/380.

2.3 | Extraction and NMR isotopic analyses

Samples were extracted with perchloric acid in liquid nitrogen, and analysed by ^{13}C-NMR as in Abadie, Lothier, Boex-Fontvieille, Carroll, & Tcherkez, 2017. The perchloric extract was neutralized, 10 and 20 μl were collected separately for LC–MS and GC–MS, respectively, and the rest was freeze-dried. LC–MS and GC–MS aliquots were frozen and spin-dried, respectively. ^{13}C-NMR analyses were performed at 298 K (25°C) without tube spinning, using an inverse-gated pulse program (zgig) with 90° pulses for ^{13}C (10 μs). Acquisition parameters were 1.3 s acquisition time, 114 k size of FID, and a relaxation delay (D1) of 15 s. 2,600 scans were done, representing about 10 hr analysis per sample. ^{13}C-signals were normalized to the internal standard (maleate).

2.4 | LC–MS analyses

LC–MS analyses were carried out as in (Abadie & Tcherkez, 2019a), using a LC–MS UHPLC/Orbitrap (Dionex/Thermo) coupling. We used a ZIC-HILIC column (3.5 μm, 200 Å, 150 × 2.1 mm, Merck SeQuant) coupled with a ZIC-HILIC column guard (20 × 2.1 mm, Merck SeQuant) at 30°C oven temperature. Samples were diluted 10 times in water/acetonitrile (vol:vol, 50:50) and an internal standard (trifluoromethyl phenylalanine, TFMP) was added to monitor the signal response of the LC–MS. For quantification, calibration curves with a mixture of standard amino acids (including TFMP) were done before, in the middle and after sample batches. Injection volume was 1 μl and elution was done at a flow rate of 0.3 ml/min with a binary gradient. Mobile phase A was acetonitrile/water (vol:vol, 25:75) and mobile phase B was acetonitrile/water (vol:vol, 95:5) both with ammonium acetate (5 mM). The gradient applied was 72% B at 0 min down to 36% B at 13 min and maintained for 2 min, and then back to 72% B at 16 min (total run time of 21 min). MS analysis was done in positive mode using two different runs: full MS scan mode (to extract metabolic features) and all ion fragmentation (AIF). The latter allowed us to look at the isotopic enrichment in fragments or check molecule identity. In fact, exact mass LC–MS data give direct access to isotopic abundances since ^{13}C isotopologues can be easily distinguished from ^{15}N, ^{2}H or ^{18}O isotopologues and thus the $\%^{13}C$ can be calculated.

2.5 | GC–MS analyses

GC–MS analyses were carried out as in (Abadie, Blanchet, et al., 2017), using gas chromatography coupled to mass spectrometry (GC–MS), via methanol: water extraction followed by derivatization with methoxylamine and *N*-methyl-*N*-(trimethylsilyl) trifluoroacet amide (MSTFA) in pyridine. Alkanes were used in each sample to compute the retention index. Signals were normalized by the internal standard (ribitol).

2.6 | Data extraction

In what follows, non-targeted analysis leads to the extraction and utilization (for statistics) of "features." This term (used broadly in metabolomics) refers to a trait that can be treated as an individual metabolic quantitative variable. In NMR, LC–MS and GC–MS a feature is a ^{13}C-signal referred to by its chemical shift, an m/z + retention time couple, and an m/z + retention index couple, respectively.

NMR spectra were phased, background corrected and retrieved from TopSpin 4.0. They were then analysed using the NMRProcFlow web application (Jacob, Deborde, Lefebvre, Maucourt, & Moing, 2017) where baseline correction (qNMR/soft) was performed. The bin area method was used to segment spectra between 11 and 185 ppm using the intelligent variable size bucketing included in NMRProcFlow. Buckets corresponding to one metabolite were then grouped when possible, according to NMR signal assignment (that is, buckets were optimized to contain entire peaks and avoid peaks being split in two subsequent buckets). A total of 181 variables were thus retained for subsequent statistical analyses. Integrated regions were normalized by dividing their areas by that of the internal standard (maleate) and dry mass of the sample.

LC–MS data were automatically aligned and features (m/z + retention time couples) were extracted with Mzmine 2 (Pluskal et al., 2020). Briefly, the raw dataset (.raw) was first converted to the mzML format (using MSConvert) and imported to Mzmine 2. Data processing started with peak detection followed by extraction of ion chromatograms (EICs) using the module Chromatogram Builder (minimum highest intensity set at 10^4 and m/z tolerance at 10^{-4} g/mol) from automated data analysis pipeline (ADAP) (Myers, Sumner, Li,

Barnes, & Du, 2017). To detect peaks from EIC chromatograms, deconvolution was performed with the wavelets algorithm, then identified peaks were aligned using the ADAP module Join Aligner using a RT and m/z tolerance of 0.05 min and 10^{-4} g/mol, respectively. LC–MS data extraction generated 39,595 features. Those with more than 50% missing data (non-detected signal in more and 50% of samples) were discarded, reducing the number of used features to 3,860. Identification of m/z features (Table 1) was based on exact mass, fragments (when visible with AIF analysis), and the isotopic pattern at natural abundance (non-labelled samples), and comparison with authentic standards (for common metabolites). In particular, when identified compounds contained sulfur, we checked the isotopic pattern comprised a ^{34}S isotopologue at natural abundance (4.3%). When identifications were nevertheless ambiguous (several possibilities), possibilities found in PubChem (https://pubchem.ncbi.nlm.nih.gov) were filtered according to biological relevance (recognized occurrence in plants). When several possible identifications were still possible, they are listed in Table 1, with the letter "A."

GC–MS data were aligned and extracted (m/z + retention index couples) using Metabolome Express (Carroll, Badger, & Millar, 2010), generating 1,574 metabolic features. In the data presented in figures, GC–MS features that were simultaneously insignificant in univariate analysis and non-identified by Metabolome Express were discarded, so that 384 features were eventually used.

2.7 | Statistics

Considering the very high number of metabolic features to be handled, it was necessary to carry out multivariate analyses to operate a dimensionality reduction in addition to classical univariate analyses. To explore the CO_2 and O_2 effect, univariate statistics were conducted with a two-way ANOVA, with one factor representing labelling (^{12}C or ^{13}C conditions) while the second factor was O_2/CO_2. Statistical significance was considered when $p < .05$, $p < .01$ or using the Bonferroni threshold (to correct for the false discovery rate), as shown in figures. Multivariate statistics were carried out using orthogonal projection on latent structure (OPLS; with Simca, Umetrics) using labelling as a qualitative (binary) Y variable and O_2/CO_2 as a quantitative Y variable, and metabolic features as predicting X variables. Before running the OPLS, a PCA was conducted to check the presence of outliers (samples outside the Hotelling's ellipse). The performance of the OPLS was assessed using the correlation coefficient between predicted and observed Y (R^2), the cross-validated correlation coefficient (Q^2), the Q^2 intercept of the permutation test (that was checked to be negative), and the p value of testing the OPLS model against a random-error model (i.e., average ± error) via a χ^2 test (this p value is referred to as $P_{CV\text{-}ANOVA}$) (Bylesjö et al., 2006; Eriksson, Trygg, & Wold, 2008). Univariate and multivariate analyses were combined using –log(p value) (univariate) plotted against the OPLS loading (p_{corr}) in a "volcano plot." In such a representation, best metabolic markers are at the extremity of the plot (upper left and upper right).

3 | RESULTS

3.1 | ^{13}C incorporation detected by NMR

As expected, the amount of CO_2 assimilated increased with the CO_2-to-O_2 ratio, while under 0% O_2 (100% N_2) as a background gas, there was a slight decline in net assimilation due to hypoxia (Figure S2). Allocation to major ^{13}C pools was analysed by NMR, which is effectively highly quantitative but rather insensitive. Individual ^{13}C signals obtained from bucketing were treated as quantitative variable. Here, each feature represents a C-atom position characterized by a chemical shift. Some C-atom positions are represented by several points due to spin–spin interactions that generate multiplets. Figure 1 shows the volcano plot combining univariate and multivariate analyses. The multivariate analysis yielded significant OPLS model ($P_{CV\text{-}ANOVA}$ = .028 for the O_2/CO_2 effect) that was both predictive (R^2 = .809) and robust (Q^2 = .752). Unsurprisingly, most features that significantly responded negatively to the O_2-to-CO_2 ratio were C-atom positions in sugars (with, for example, a p value smaller than 10^{-9} for the C-2 atom position in β-fructose) while photorespiratory intermediates (glycine, serine, glycerate) were more labelled at low carboxylation (high O_2/CO_2).

Several C-atom positions in amino acids were also significantly related to O_2/CO_2, in alanine or (*iso*)leucine. Accordingly, an intermediate of leucine metabolism (oxoisovalerate) was more labelled at high O_2/CO_2. The C-5 atom of methionine appears just above the threshold of p = .05, either negatively related (native methionine) or positively correlated (methionine sulfoxide) to O_2/CO_2 reflecting the complicated pattern of ^{13}C-5 in methionine: on the one hand, high photosynthesis (low O_2/CO_2) increased ^{13}C-labelling (^{13}C input) but on the other hand, methionine biosynthesis was stimulated by photorespiratory conditions (high O_2/CO_2). As a matter of fact, another C-atom position of methionine (C-2) and *O*-succinylhomoserine (C-3) appeared to be more labelled at high O_2/CO_2. Interestingly, the ^{13}C-signal of C-atom positions in several organic acids also appeared to be significantly higher at high O_2/CO_2: malate (C-1, C-3 and C-4), citrate (C-2/4) and isocitrate (C-3) and fumarate (C-1/4), with malate C-4 having the lowest p value (10^{-8}). This strongly suggests an increase in both catabolism via the tricarboxylic acid pathway and bicarbonate fixation (onto C-4 of oxaloacetate and thus malate) when photorespiration is high. We also note that the ^{13}C-signal of chlorogenate (caffeoylquinate) C-3/7 was significantly higher at high O_2/CO_2.

3.2 | Metabolic features observed by mass spectrometry

Volcano plots associated with GC–MS and LC–MS features are presented in Figures 2 and 3, respectively. Excellent correlation was observed between observed Y values and Y values predicted by the statistical OPLS model (Figure S3). Here, features represent molecular species (isotopologues of metabolites). The multivariate analysis with GC–MS features yielded a significant OPLS model ($P_{CV\text{-}ANOVA}$ = .009 for the O_2/CO_2 effect) that was both predictive (R^2 = .906) and robust

TABLE 1 List of *m/z* ions observed in LC–MS and significant for the O_2/CO_2 effect (Bonferroni threshold, –log(*p*) > 4.88)

#	Index	*m/z*	RT (min)	p(corr)	VIP	–log(*p*)		Identification
1	3,980	369.158	3.003	−0.215	1.074	*		$^{13}C_1$-*N*-valyladenosine.H^+
2	3,757	352.207	3.174	−0.070	0.950	15.955	A	*N*-lauroylglutamic acid.Na^+ Glucosylheliotridine.NH_3.NH_4^+
3	3,099	310.128	2.611	−0.168	2.044	15.477	A	Methionylmethionine sulfoxide–H_2O.Form.NH_4^+ *N*-citryl diaminobutyric acid.NH_4^+
4	2,626	282.144	3.881	0.028	0.617	15.353		$^{13}C_2$-Glucosylvaline.H^+
5	924	168.065	3.682	−0.134	1.348	14.364		Methionine.H_2O.H^+
6	3,644	344.133	3.912	0.132	0.582	14.142	A	Glucosyltyrosine.H^+ Glucosylhydroxycinnamic acid.NH_4^+
7	3,134	312.111	3.355	−0.049	1.797	13.509		*N*-fructosylmethionine.H^+
8	1940	239.095	7.821	−0.798	2.406	10.752		$^{13}C_1$-Fructosylglycine.H^+
9	8,245	372.189	4.690	0.360	2.930	9.214		$^{13}C_{12}$-Sucrose.NH_4^+
10	2,294	262.128	3.879	0.102	1.010	8.944		Galactaric acid.2NH_3.NH_4^+
11	4,243	388.109	10.484	0.051	1.400	8.291		$^{13}C_1$-Dihydroxycinnamoyl-pentosylglucosylflavanone.2H^+
12	1,124	183.129	1.458	−0.293	0.494	8.251		$^{13}C_2$-Adipic acid.NH_3.NH_4^+ $^{13}C_2$-Quinovosamine.NH_4^+
13	185	90.055	5.321	0.616	1.788	8.198		Alanine.H^+
14	7,117	240.098	7.825	−0.628	2.234	6.698		$^{13}C_2$-Fructosylglycine
15	1,106	182.081	3.433	0.627	1.300	6.680		Tyrosine.H^+
16	572	136.076	3.432	0.620	1.288	6.567		$^{13}C_4$-δ aminolevulinic acid.H^+
17	1,303	197.053	2.494	−0.477	1.400	6.322		Gluconic acid.H^+
18	1,119	183.084	3.431	0.596	1.265	6.277		$^{13}C_1$-Tyrosine.H^+
19	3,226	317.208	1.245	−0.053	1.135	6.238	U	Unknown S-containing compound (probable formula $C_{16}H_{32}N_2S_2$)
20	10,845	337.196	1.973	−0.089	1.057	6.198	U	Unknown sugar derivative (probable formula $C_{14}H_{28}N_2O_7$)
21	10,328	261.048	3.554	−0.177	0.645	6.129		Deoxyxylulose 5-phosphate.NH_3.NH_4^+
22	877	164.071	2.035	−0.297	1.135	6.076		Aminocinnamic acid.H^+
23	4,536	411.362	1.272	−0.028	0.277	5.673	U	Unknown
24	2,554	278.149	3.157	−0.263	0.654	5.671	A	$^{13}C_2$-Butylglucose.NH_3.Na^+ $^{13}C_2$-Methylglucaric acid.2NH_3.NH_4^+ $^{13}C_2$-Ketoheptulose.2NH_3.NH_4^+
25	4,678	425.192	1.738	−0.264	0.481	5.620		Glucosylresveratrol.NH_4^+
26	5,799	588.158	9.955	−0.404	1.228	5.599	A	$^{13}C_2$-Phosphocaffeoylpentoglucoside.NH_4^+ $^{13}C_2$-Phosphoferuloylxyloglucan.NH_4^+
27	1,349	200.092	3.880	−0.153	1.271	5.377		Homovanillic acid.NH_4^+
28	4,539	412.145	2.816	−0.350	1.678	5.319	A	Dihydroquercetin.5H_2O.NH_4^+ Triacetylinosine.NH_4^+ Methylgalactoglucuronic acid.ACN.H^+
29	10,095	230.042	2.130	0.029	0.413	5.268		Sulfonoasparagine.NH_4^+
30	3,404	329.142	2.608	−0.238	1.675	5.198		$^{13}C_1$-*O*-glucosylcinnamic acid.NH_4^+
31	3,746	351.176	2.014	−0.204	2.020	4.905	A	Benzylglucose.NH_3.Form.NH_4^+ Hexitollysine.Na^+ (Aminoheptanoic acid)$_2$.H^+

Note: A positive (resp. negative) value of p(corr) indicates the ion of interest prevails under low (resp. high) O_2/CO_2. When no isotope is mentioned, the compound shown refers to the monoisotopic (^{12}C) form. Formic acid is abbreviated "Form." Neutral losses are indicated with a minus sign (–). Combination with another molecule appears with a dot point (.). All *m/z* have been observed in positive ionization mode and appeared as $[M + H]^+$ ions or an adduct (in most cases, ammonium). For clarity, this table only shows 3 decimals for *m/z* (while the analysis at high resolution gave access to 5 decimals). The asterisk (*) indicate a non-computable *p* value (with ANOVA) due to the ion of interest disappearing specifically in one condition. "#" (left column) refers to the label in Figure 2. Letters "A" and "U" indicate features with several possible identifications or unknown (not identified) compounds, respectively. LC–MS features significant for the interaction effect (labelling × O_2/CO_2) are listed in Table S2.

Abbreviations: p(corr), loading associated with labelling as a response variable in OPLS; RT, retention time; VIP, variable importance for the projection.

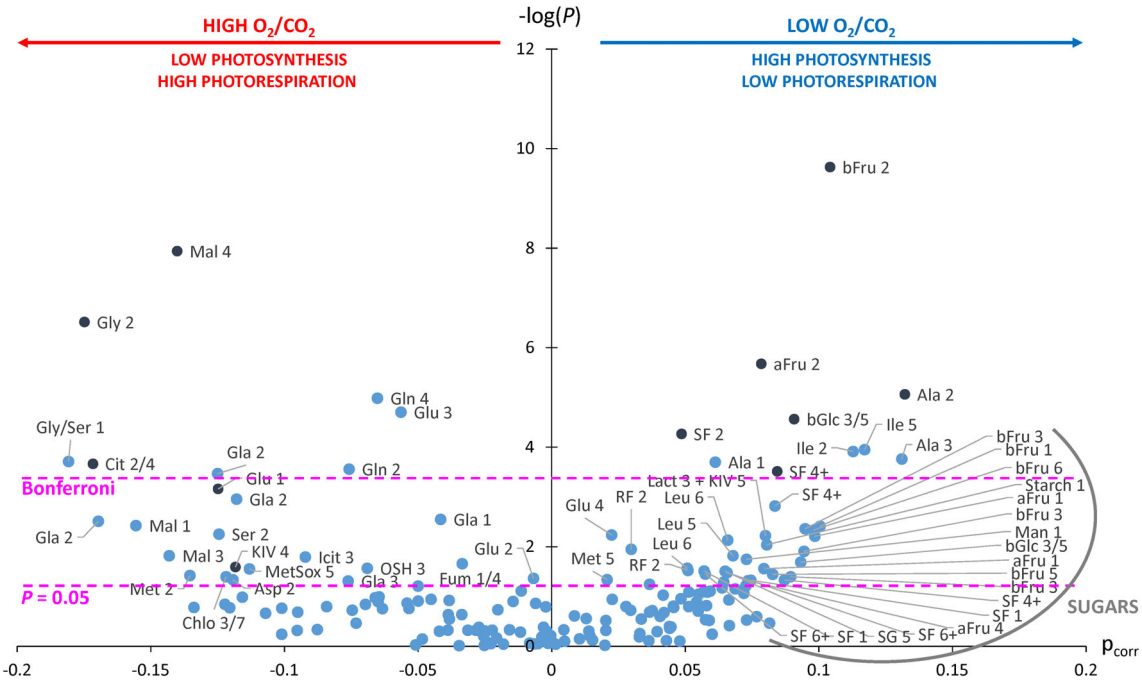

FIGURE 1 Volcano plot showing ^{13}C-signals that vary significantly with gas exchange conditions using non-targeted ^{13}C-NMR analysis. This figure plots the logarithm of the *p* value obtained in univariate analysis (two-way ANOVA, *y* axis) as a function of the weight obtained in multivariate analysis (O2PLS, *x*-axis). C-atom position associated with a significant interaction effect (labelling × O_2/CO_2) appear in dark blue. C-atom positions are named after the abbreviation of the metabolite followed by the C-atom number (IUPAC numbering). Amino acids are abbreviated using their international three-letter code. Chlo, chrorogenate; Cit, citrate; aFru, α-fructose; bFru, β-fructose; Fum, fumarate; Gla, glycerate; aGlc, α-glucose; bGlc, β-glucose; Icit, isocitrate; KIV, oxoisovalerate; Lact, lactate; Mal, malate; Man, mannose; MetSox, methionine sulfoxide; OSH, *O*-succinylhomoserine; RF, raffinose fructosyl moiety; SF, sucrose fructosyl moiety; SG, sucrose glucosyl moiety. The symbol + indicates overlapping with other sugars: due to ^{13}C-^{13}C interactions, several C-atom positions overlap at the same chemical shift. Under such circumstances, labels indicated here refer to the prevalent sugar species at the chemical shift of interest. "Starch" refers to soluble amylopectin. Note that the two CH_3 groups in leucine are distinguishable by NMR due to heterotopicity; here they are numbered as Leu 5 and 6 [Colour figure can be viewed at wileyonlinelibrary.com]

(Q^2 = 0.734). The OPLS model with LC–MS feature was, as expected, highly predictive but insignificant ($P_{CV\text{-}ANOVA}$ = .195) due to the very high number of features which causes multivariate overfitting. Typically, when this effect was partly withdrawn by eliminating features with very low p_{corr} values (first quartile), the OPLS model was significant ($P_{CV\text{-}ANOVA}$ = .041 for the O_2/CO_2 effect), highly predictive (R^2 = .996), and robust (Q^2 = 0.536).

As with NMR, most metabolic features found by GC–MS and significantly related to O_2/CO_2 were sugars ^{13}C-isotopologues, with many multiple labelled species (e.g., $^{13}C_6$- and $^{13}C_7$-sucrose). However, best features also included phosphorylated sugars (ribose 5-phosphate, glucose 6-phosphate and mannose 6-phosphate), disaccharides other than sucrose (cellobiose, maltose), myoinositol and raffinose. Interestingly, represented features were not only ^{13}C-isotopologues but also monoisotopic forms (^{12}C isotopologues) of mannose 6-phosphate, sucrose and maltose, demonstrating that both the ^{13}C-enrichment and pool size increased with net photosynthesis (in contrast to ^{12}C-galactinol, which decreased). Several amino acid isotopologues declined significantly with O_2/CO_2 such as valine, tyrosine, γ-aminobutyrate (GABA) and alanine. Here too, ^{12}C-isotopologues were represented, showing a decrease in pool size. Interestingly, high O_2/CO_2 was associated with a higher ^{13}C-labelling in quinate (increase in $^{13}C_1$-quinate, and decrease in ^{12}C-quinate), a precursor of chlorogenate.

Significant metabolic features found by LC–MS were consistent with that found by GC–MS (Figure 3), with alanine, valine (or its glycosylated derivative), tyrosine and sucrose isotopologues being more prevalent at low O_2/CO_2 (the list of features significantly affected by the ^{12}C/^{13}C substitution is shown in Table S1, and the list of features significantly affected by O_2/CO_2 is provided in Table 1). Conversely, at high O_2/CO_2, there was more methionine (and other metabolites of sulphur metabolism: *N*-fructosylmethionine, sulfonoasparagine), an intermediate of lysine metabolism (aminoadipate) and many phenylpropanoids (including glycosylated forms), as either ^{12}C or ^{13}C isotopologues.

3.3 | Isotopic forms of selected metabolites

As expected, the %^{13}C in photorespiratory intermediates serine and glycine increased as O_2/CO_2 increased, with a progressive decline in the ^{12}C-isotopologue (Figure S4). It is worth noting that the $^{13}C_3$

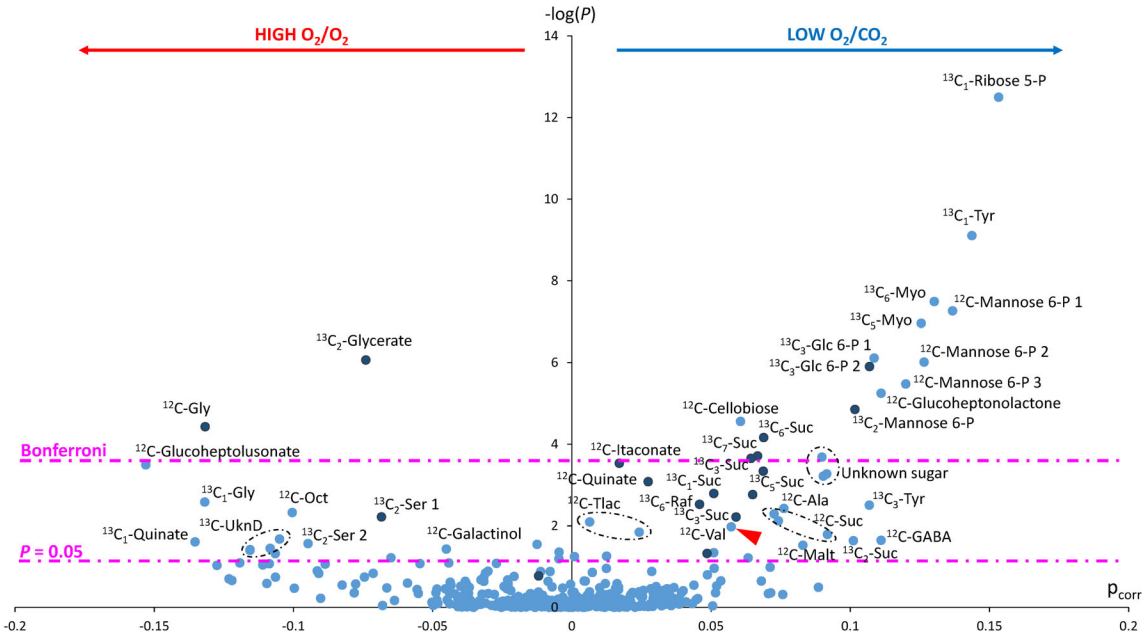

FIGURE 2 Volcano plot showing features that vary significantly with gas exchange conditions using non-targeted GC–MS analysis. This figure plots the logarithm of the *p* value obtained in univariate analysis (two-way ANOVA, *y* axis) as a function of the weight obtained in multivariate analysis (O2PLS, *x*-axis). Features associated with a significant interaction effect (labelling × O_2/CO_2) appear in dark blue. The red arrow points to valine, which is further discussed in main text. Amino acids are abbreviated using the international three-letter code. Numbers next to metabolites names refer to different analytes (different silylated derivatives). Ala, alanine; GABA, γ-aminobutyrate; Glc, glucose; Gly, glycine; Malt, maltose; Myo, myoinositol; Oct, octacosane; Raf, raffinose; Ser, serine; Suc, sucrose; Tlac, threonolactone; Tyr, tyrosine; UknD, unknown disaccharide (sucrose isomer to be determined); Val, valine [Colour figure can be viewed at wileyonlinelibrary.com]

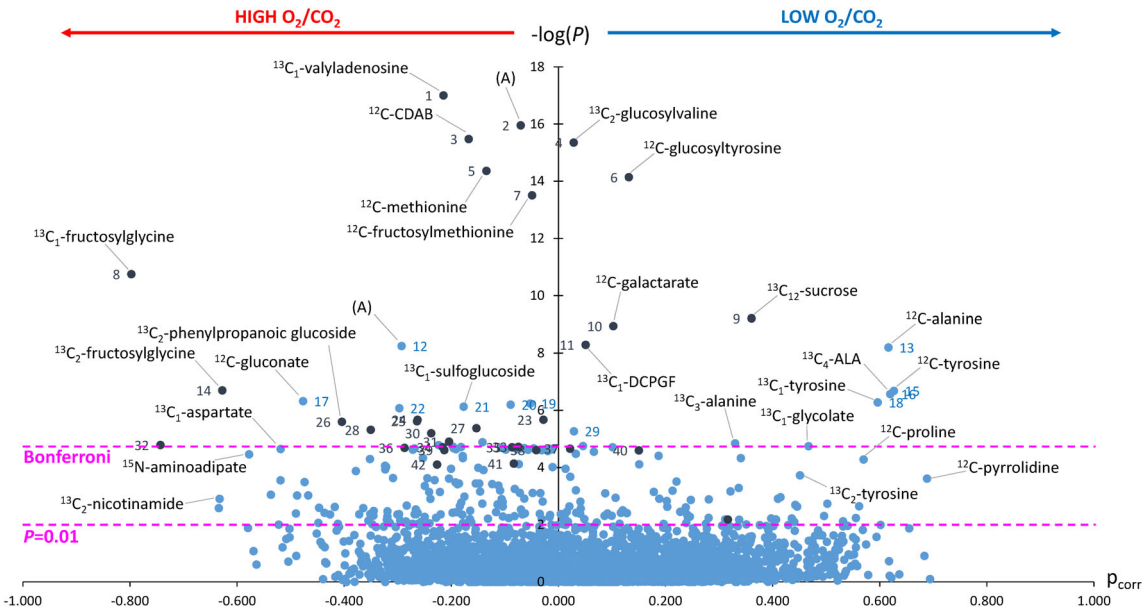

FIGURE 3 Metabolites affected by O_2/CO_2 and detected by LC–MS. Volcano plot showing *m/z* features that vary significantly with gas exchange conditions using non-targeted LC–MS analysis. This figure plots the logarithm of the *p* value obtained in univariate analysis (two-way ANOVA, *y* axis) as a function of the weight obtained in multivariate analysis (O2PLS, *x*-axis). *m/z* associated with a significant interaction effect (labelling × O_2/CO_2) appear in dark blue. For each feature, the isotopologue is indicated (number of ^{13}C atoms). Monoisotopic ions (with no heavy isotopic substitution) are indicated as "^{12}C." Number refers to the compound number in Tables 1 and S2 (where the exact mass and adduct forms are indicated). ALA, δ-aminolevulinic acid; CDAB, citryldiaminobutyrate; DCPGF, dihydroxycinnamoyl pentosylglucosyl flavanone. The symbol (A) indicates several possibilities for identification (see tables) [Colour figure can be viewed at wileyonlinelibrary.com]

isotopologue of serine was not maximal at the highest O_2/CO_2 (100% O_2 as background gas) because of the low ^{13}C input by photosynthesis.

Since O_2/CO_2 impacted on branched chain amino acids, phenylpropanoids and sulphur assimilation, we looked more closely at the isotopic distribution in valine, phenylalanine and methionine (Figure 4). Valine appeared to be minimally labelled under 100% O_2 as a background gas (Figure 4b). There were also clear changes in the isotopic pattern. The $^{13}C_1$-isotopologue always represented between 5 and 6%, reflecting ^{13}C natural abundance (1.1% × number of C-atoms, here, 5) (Figure 4c). When valine was labelled, this was mostly due to the occurrence of the completely labelled isotopologue, $^{13}C_5$-valine, demonstrating that acetyl-CoA and pyruvate used to synthesize valine were maximally labelled.

The isotopic pattern was very different in phenylalanine compared to valine. In fact, the two prevalent isotopologues were $^{13}C_3$- and $^{13}C_9$-phenylalanine (except at high O_2/CO_2 where phenylalanine was minimally labelled) (Figure 4f). Since phenylalanine C-atoms come from two PEP and one erythrose 4-phosphate (E4P) molecule, it shows that the two most common situations were $^{13}C_3$-PEP + ^{12}C-PEP + ^{12}C-E4P ($^{13}C_3$) and 2 × $^{13}C_3$-PEP + $^{13}C_4$-E4P ($^{13}C_9$). In other words, it suggests the involvement of two pools of shikimate, one being strongly labelled, while the other was minimally labelled. This dual origin persisted regardless of O_2/CO_2 except under 100% O_2 (Figure 4f).

In the case of methionine, there was a very clear predominance of the $^{13}C_1$-isotopologue (20–30%), far above natural abundance (1.1% × 5) (Figure 4i), demonstrating the strong labelling in methyl-THF

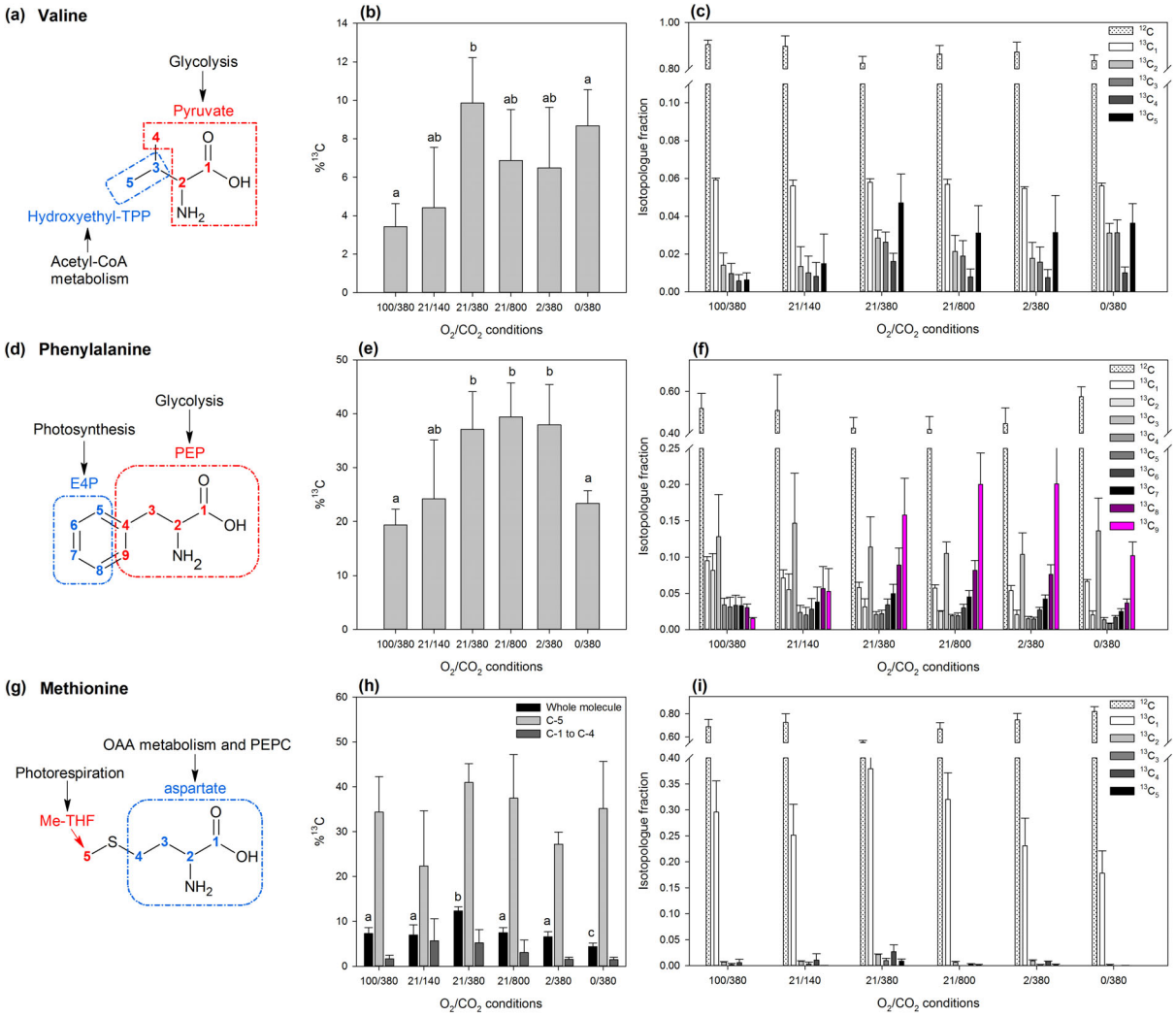

FIGURE 4 Isotopic pattern in selected amino acids of sunflower leaves labelled with $^{13}CO_2$: (a–c) valine, (d and f) phenylalanine and (g–i) methionine. (a,d,g) Chemical structure of amino acids showing their metabolic origin. "Photosynthesis" refers to the Calvin cycle that generates pentose phosphates. Me-THF, methyl-tetrahydrofolate; OAA, oxaloacetate; PEPC, phospho*enol*pyruvate carboxylase; TPP, thiamine pyrophosphate. (b,e,h) ^{13}C percentage from full MS (and for methionine, also fragmentation analysis). Letters stand for statistical classes ($p < .05$, ANOVA). (c,f,i) Isotopologue distribution showing that the isotopic pattern is far from being statistical, with a very high proportion of $^{13}C_5$ isotopologues (valine), both $^{13}C_3$ and $^{13}C_9$ isotopologues (phenylalanine) and $^{13}C_1$ isotopologue (methionine) [Colour figure can be viewed at wileyonlinelibrary.com]

from which the CH_3 group attached to the S-atom comes. The use of LC–MS fragments that do not comprise the CH_3 group allowed us to compute by subtraction the $\%^{13}C$ in the non-methyl atoms of methionine. The C-atoms coming from aspartate were effectively much less labelled than the methyl group (Figure 4h,i).

In addition, of particular interest is the isotope composition in adenosine which is among the most significant labelled compounds and is neither an amino acid nor a sugar (Table S1). In addition, the $^{13}C_1$ isotopologue of valyladenosine was the most significant LC–MS feature associated with the O_2/CO_2 effect (Table 1 and Figure 3). There were no significant changes in the adenosine pool size (Figure 5b); however, its $\%^{13}C$ varied significantly, with the lowest value at low O_2/CO_2 that is, with 0% O_2 as a background gas (Figure 5c). The isotopic pattern was far from being statistical, with a

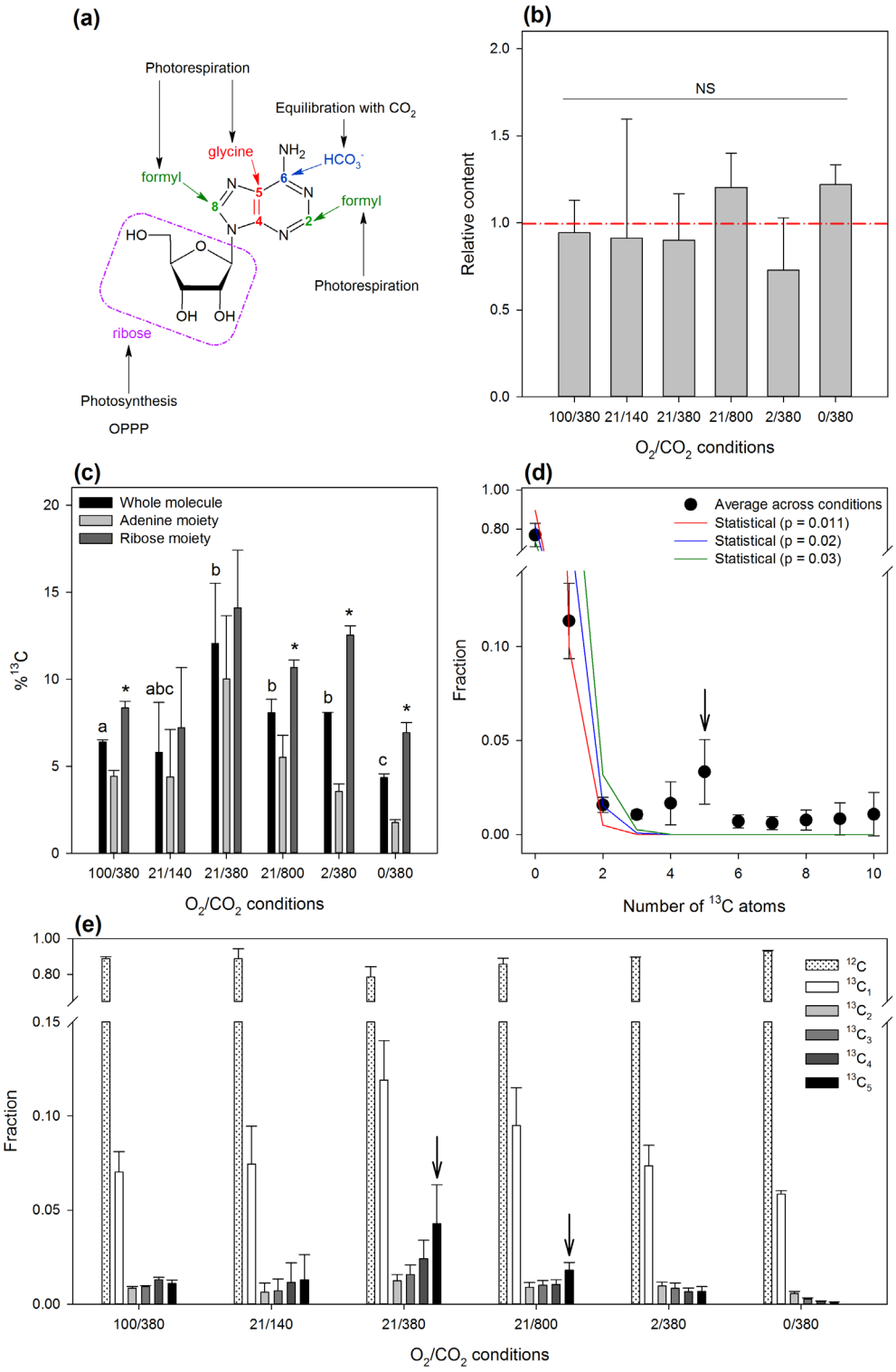

FIGURE 5 Isotopic pattern in adenosine of sunflower leaves labelled with $^{13}CO_2$. (a) Chemical structure of adenosine and origin of C-atoms. Here, "formyl" refers to formyl-tetrahydrofolate. The term "photosynthesis" refers to the Calvin cycle that forms pentoses. (b) Relative content in adenosine. The red line indicates the relative average across all conditions, fixed at 1. There is no significant difference between conditions. (c) ^{13}C percentage of whole molecule (obtained from full MS analysis) and of the adenine moiety (obtained from fragmentation) and the ribose moiety (calculated from mass balance). (d) Average mole fraction of isotopologues (across all O_2/CO_2 conditions) of adenosine (black dots) and comparison with purely statistical ^{13}C distribution with a one-^{13}C probability of 0.011 (natural abundance, red)), 0.02 (blue) or 0.03 (green). The arrow points towards the remarkably high fraction associated with the $^{13}C_5$ isotopologue. (e) Isotopologue distribution (mole fraction) in the adenine moiety of adenosine. Arrows point to the high proportion of fully labelled ($^{13}C_5$) adenine molecules. Data shown are $M \pm SD$ ($n = 3$). OPPP, oxidative pentose phosphate pathway [Colour figure can be viewed at wileyonlinelibrary.com]

high proportion of the $^{13}C_5$ isotopologue, simply reflecting the high ^{13}C labelling in the ribosyl moiety (Figure 5d, arrow). The isotope composition of the adenine moiety was then examined precisely using the associated fragment in LC–MS AIF analysis. The isotopic pattern was not statistical, with a high contribution of the $^{13}C_5$ isotopologue at 380 and 800 μmol/mol CO_2 in 21% O_2 (Figure 5e). Interestingly, this isotopologue remained relatively important even at high O_2/CO_2 (100% O_2) while it nearly disappeared at low O_2/CO_2 (0% O_2), suggesting that the allocation of ^{13}C to adenosine biosynthesis was very small when photorespiration was suppressed.

4 | DISCUSSION

The overall metabolic impact of changing CO_2 and O_2 conditions during gas exchange has never been described precisely using comprehensive metabolic analyses. Here, we provide the first non-targeted isotope-assisted analysis to find the most important metabolic changes, beyond carboxylation and oxygenation. The most visible changes we found were associated with PEPC activity, sulphur assimilation and phenylpropanoids (stimulated at high photorespiration), branched chain and tyrosine synthesis (stimulated at high photosynthesis). The effect of hypoxia on leaf alanine metabolism has been previously discussed (Abadie, Blanchet, et al., 2017) and will not be commented further here. In what follows, we discuss the possible rationale for metabolic modifications (in particular in relation to photorespiration) and potential consequences for gas exchange measurements themselves (in particular for day respiration).

4.1 | Reconfiguration of amino acid metabolism

One of the most significant impact of O_2/CO_2 conditions was the enhancement of methionine metabolism, with not only an increase in the methionine pool (Tables 1, 2, & Figure 3a) but also a higher ^{13}C allocation to methionine sulfoxide and *O*-succinylhomoserine at high O_2/CO_2 (Figure 1). Interestingly, the ^{13}C enrichment in methionine was much more pronounced in the C-5 atom, that is, the methyl group attached to S, which comes from C_1 metabolism. By contrast, the ^{13}C enrichment in other C-atoms was small, showing that the allocation of ^{13}C-aspartate to methionine de novo synthesis was modest. The considerable ^{13}C enrichment in C-5 at high photorespiration despite the low ^{13}C input (low net assimilation) demonstrates the critical role of photorespiration-derived methyl-THF in providing the C_1 unit to convert homocysteine to methionine (the final step of methionine synthesis) (Hanson & Roje, 2001). Similar results have been obtained recently also on sunflower leaves (Abadie & Tcherkez, 2019b), where the effect of photorespiratory conditions on methionine was further shown with ^{33}S-labelling to be accompanied by an increase in sulphate reduction and assimilation. Taken as a whole, this shows the stimulation of sulphur metabolism at high O_2/CO_2. This effect is here further supported by the significant effect on sulphur-containing metabolites other than methionine, such as *N*-fructosyl methionine, and sulfonoasparagine (Table 1, Figure 3).

More generally, our data support the view that aspartate metabolism as a whole is stimulated by high O_2/CO_2 conditions, as suggested by the significantly higher ^{13}C-signal in aspartate itself (Figure 1) and nicotinamide (Figure 3) and the clear stimulation of PEPC activity (which generates oxaloacetate; discussed below). In addition, our results suggest a higher flux in lysine metabolism (synthesis + degradation), which starts from aspartate and leads to aminoadipate (and then 2-oxoglutarate) via aminopimelate and lysine. Here, we found an increase in the pool of aminoadipate (Figure 3). Interestingly, the involvement of the lysine bypass has also been demonstrated in *Arabidopsis* mutants affected in isocitrate dehydrogenase (NADP and NAD dependent) activity (Boex-Fontvieille, Gauthier, Gilard, Hodges, & Tcherkez, 2013). Such a similarity perhaps reflects the higher redox poise in the mitochondrion at high photorespiration rates due to high NADH generation by glycine-to-serine conversion. That is, under such circumstances, the lysine bypass would be up-regulated to play the role of an alternative pathway to supplement 2-oxogluratate generation.

Another clear effect of O_2/CO_2 conditions is the modification of phenylpropanoids metabolism. In fact, while there was an increase in ^{13}C- and ^{12}C-tyrosine signals at high photosynthesis (low O_2/CO_2), there was an increase in non-aminated derivatives at high photorespiration (high O_2/CO_2) such as chlorogenate and its precursor quinate (^{13}C-isotopologue, while the ^{12}C-isotopologue decreased thus demonstrating an enhanced turn-over) (Figure 3), and other metabolites of this family such as phosphocaffeoylpentoglucoside, homovanillate and amino- and glucosyl-cinnamate (Table 1). In other words, the metabolic partitioning of the aromatic precursor arogenate appears to change depending on O_2/CO_2: at high O_2/CO_2, the synthesis of secondary metabolites via phenylalanine is favoured while at low O_2/CO_2, tyrosine synthesis is favoured. It is worth noting that phenylalanine itself was not amongst significant features (Figures 1–3) suggesting that it played the role of an intermediate that did not accumulate (while its isotopic enrichment can be very high, up to ≈40%, Figure 4). In addition, the isotopic pattern found in phenylalanine was quite surprising, in that the two predominant isotopologues were $^{13}C_3$ and $^{13}C_9$, strongly suggesting that phenylalanine synthesis could remobilize non-labelled shikimate and therefore, there were two pools of shikimate in the cell (chloroplastic and extra-chloroplastic). Alternatively, there could be some de novo shikimate synthesis from non-labelled precursors (PEP, E4P) in the cytosol. In both cases, non-labelled shikimate has to be imported into the chloroplast (Maeda & Dudareva, 2012). The utilization of shikimate appeared to be enhanced at high O_2/CO_2 (Figure 4f). The rationale of the phenylalanine derivatives vs. tyrosine balance when O_2/CO_2 conditions change is not clear. Promoting secondary metabolites (coming from phenylalanine) over tyrosine has some advantages at high photorespiration: First, it liberates ammonium (via phenylalanine ammonia lyase, PAL) which is then available for the GS-GOGAT cycle and can thus feed the photorespiratory cycle with glutamate. Second, since PAL is cytosolic (as well as other enzymes of caffeate synthesis), it eventually

TABLE 2 Overall chemical equations of metabolic phenomena mentioned in Figure 6, showing the potential impact on CO_2 exchange, via the fixation or production of CO_2 (or bicarbonate in the case of PEPC)

Metabolic pathway	Summarized reaction	Consequences on net CO_2 exchange
Anaplerosis	PEP + $\mathbf{HCO_3^-}$ → oxaloacetate	Consumes HCO_3^-
Hypoxic metabolism (alanine production + GABA shunt)	Pyruvate + Glu → Ala + SSA + $\mathbf{CO_2}$	CO_2 production via GABA synthesis (but pyruvate abstraction from catabolism)
Aspartate metabolism	Asp +2 ATP → Thr + 2 ADP + 2 Pi Asp + Cys + Me-THF + 2 ATP → Met +2 ADP + 2 Pi + pyruvate Asp + pyruvate + Glu → $\mathbf{CO_2}$ + 2OG + Lys, and Lys + 2OG → $\mathbf{CO_2}$ + 2 Glu	Consumes HCO_3^- (via asp synthesis); Cys synthesis utilizes photorespiratory Ser; CO_2 production during Lys metabolism (but pyruvate abstraction from catabolism)
Adenosine synthesis	Ribose 5-P + 2 Fo-THF + 6 ATP + 2 Gln + Gly + $\mathbf{HCO_3^-}$ + Asp → adenosine +2 THF + 7 Pi + 5 ADP + AMP + 2 Glu + fumarate	Consumes 2 HCO_3^- (one of them via asp synthesis)
Branched chain amino acid synthesis	2 Pyruvate + Glu → Val + $\mathbf{CO_2}$ + 2OG Pyruvate + Thr + Glu → Ile + $\mathbf{CO_2}$ + 2OG 3 Pyruvate + Glu → Leu + 2 $\mathbf{CO_2}$ + 2OG	CO_2 production (but pyruvate abstraction from catabolism)
Phenylpropanoid metabolism	2 PEP + erythrose 4-P + Glu + ATP → Phe (or Tyr) + 2OG + 4 Pi + ADP + $\mathbf{CO_2}$	CO_2 production and PEP abstraction from anaplerotic activity

Note: For simplicity, redox equivalents (NADPH, NADH) are not mentioned here. Amino acids are abbreviated using the international three-letter code. Abbreviations: 2OG, 2-oxoglutarate; PEP, phospho*enol*pyruvate; SSA, succinic semialdehyde; THF, tetrahydrofolate.

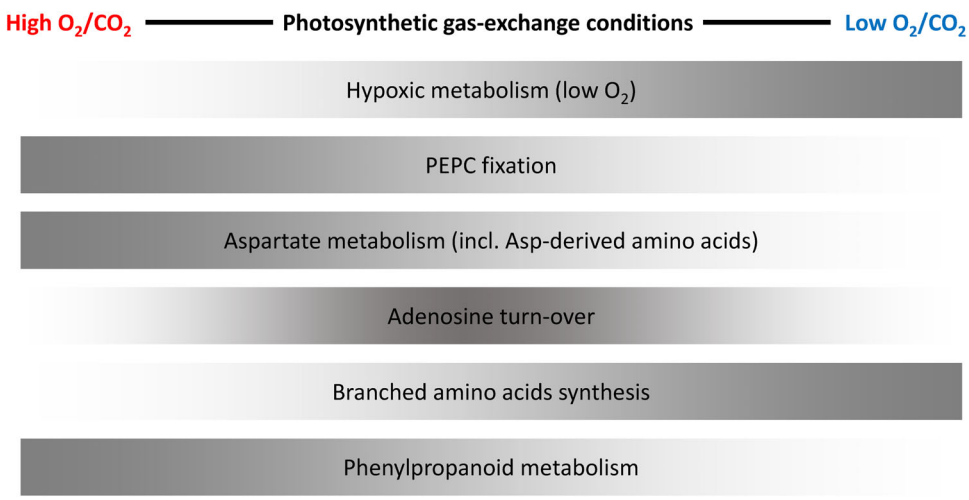

FIGURE 6 Summary of metabolic pathways affected by gas exchange O_2/CO_2 conditions in sunflower leaves [Colour figure can be viewed at wileyonlinelibrary.com]

leads to a net export of redox power from the chloroplast, whereas tyrosine synthesis generates NADPH in the chloroplast. Third, phenylpropanoids can play the role of antioxidants and this may be beneficial at high photorespiration (Mhamdi, Kerchev, Willems, Noctor, & Van Breusegem, 2017; Noctor & Mhamdi, 2017). In particular, lignin precursors (hydroxycinnamate family members) can participate in quenching radical ROS via monodehydroascorbate reductase (Sakihama, Ji, Sano, Asada, & Yamasaki, 2000).

O_2/CO_2 also impacted on branched chain amino acids, with an increase in the ^{13}C-signal of (glycosyl)valine, leucine, isoleucine, as well as an increase in ^{12}C-valine with net photosynthesis (Figures 1–4). The relatively high signal of the $^{13}C_5$-isotopologue of valine shows clearly that de novo synthesis took place from $^{13}C_3$-pyruvate (in the chloroplast). It is worth noting that isoleucine synthesis also involves threonine as a building block and this probably explains why threonine was not among significantly decreased metabolites at low O_2/CO_2 despite the general down-regulation of aspartate metabolism under such conditions.

4.2 | Catabolism and CO_2 production

Nearly all of the pathways that were found to vary with O_2/CO_2 are associated with CO_2 production or fixation (Figure 6 & Table 2). First, we found a stimulation of PEPC activity at high O_2/CO_2 (with a strong ^{13}C signal in malate C-4, Figure 1). As a result, bicarbonate fixation increased and providing the HCO_3^-/CO_2 equilibrium was maintained, this must have translated into higher apparent carboxylation rate. The

numerical impact of PEPC-catalysed fixation on v_c has been examined previously (Abadie & Tcherkez, 2019a). PEPC activity is essential to sustain aspartate synthesis in leaves, and aspartate metabolism is in turn stimulated at high photorespiration (see previous section). While methionine synthesis does not lead to CO_2 production, the lysine bypass from aspartate to 2-oxoglutarate generates two CO_2. Phenylalanine, tyrosine, and branched chain amino acid synthesis also produces CO_2 (Table 2).

Interestingly, adenosine synthesis, which is one of the highest significant features upon $^{13}CO_2$ labelling (and its *N*-bound valine derivative has the highest *p* value for the O_2/CO_2 effect), involves bicarbonate fixation. The ^{13}C-enrichment in the adenine moiety is bell-shaped, with a maximal value under standard conditions (Figure 5). This pattern likely comes from both a source effect (where precursors, glycine and C_1 units, are maximally labelled at high photorespiration) and a down-regulation of adenine turn-over at high photosynthesis (as demonstrated by the lower $\%^{13}C$ in the ribose moiety (Figure 5) despite its higher ^{13}C-signal (Figure 2)). Taken as a whole, adenosine de novo synthesis increased at high photorespiration and this must have increased the apparent carboxylation rate. The significance of this effect on the AMP, ADP or ATP pool size (collectively referred to as AXP) as O_2/CO_2 varies would require further analysis. De novo synthesis of purine bases is believed to take place not only in plastids but also in mitochondria while the "salvage pathway" is cytosolic (Zrenner, Stitt, Sonnewald, & Boldt, 2006). An increase in AXP turn-over could thus be useful to either (a) balance the cytosolic energetic charge ratio (ATP/AXP) or (b) adjust the capacity of ATP generation by the mitochondrion when photorespiratory NADH production increases and tends to increase the ATP/ADP ratio ((Bykova, Keerberg, Pärnik, Bauwe, & Gardeström, 2005; Gardeström & Wigge, 1988) but see (Yin, Dietz, & Heber, 1990)).

The net effect of changing O_2/CO_2 conditions on metabolic CO_2 efflux and how it contributes to R_d is not known with precision. In fact, our study did not include time series or steady-state isotopic labelling (which is not attainable), therefore numerical flux calculations were not possible. If we neglect temporal changes in pool sizes (and thus assume that pool sizes were constant), the $\%^{13}C$ values (along with external calibration) suggest that branched chain amino acid, phenylalanine + tyrosine and adenosine synthesis represent an apparent ^{13}C allocation within 0.02–0.05, 0.02–0.04 and 0.005–-0.02 μmol m^{-2} s^{-1}, respectively. Such values are small compared to photosynthesis under standard conditions (21% O_2, 380 μmol mol^{-1} CO_2) but are not negligible when compared with net photosynthesis at low CO_2 or high O_2, or with day respiration (about 0.5 μmol m^{-2} s^{-1}). In fact, it represents a total CO_2 efflux of up to 0.1 μmol m^{-2} s^{-1}, that is, up to 20% of average day respiration rate. In addition, this multiplicity of metabolic pathways associated with CO_2 exchange must be kept in mind when gas exchange measurements are carried out. That is, the generic term "day respiration" encompasses various metabolic pathways and although "classical" decarboxylation (pyruvate dehydrogenase, tricarboxylic acid pathway) likely prevails in total CO_2 efflux, variations in R_d with environmental conditions can also be partly explained by changes in minor decarboxylating pathways.

In addition, when net assimilation is low, alternative carboxylation pathways (PEPC, base synthesis) cannot be neglected. PEPC activity has been shown to be up to 1.8 μmol m^{-2} s^{-1} at high photorespiration, which is not negligible compared to net photosynthesis and implies a significant correction in calculations to compute carboxylation (v_c) and oxygenation (v_o) rates (Abadie & Tcherkez, 2019a). This situation is likely to occur when low CO_2 mole fraction is used, for example during day respiration determination with the Laisk method.

4.3 | Perspectives

Overall, the present study highlights the multiple metabolic changes that accompany the manipulation of CO_2 and O_2 mole fraction in gas exchange systems. Of course, we recognize that our experimental system was destructive and required instant sampling at each O_2/CO_2 condition of interest. It would be better to have experimental means to monitor metabolism in vivo in a non-destructive manner, so as to appreciate its contribution to non-photosynthetic and non-photorespiratory CO_2 exchange. Unfortunately, there is presently little opportunity to do so since the most adapted technique for metabolic measurements in vivo, namely NMR, is currently not adaptable to ^{13}C analysis on flat, air-filled organs like intact leaves. We also recognize that molecular mechanisms underlying the metabolic changes described here would require further analyses. In *Arabidopsis* rosettes, the change in (phospho*enol*)pyruvate metabolism with O_2/CO_2 has been shown to correlate to phosphorylation of, for example, PEPC (Abadie et al., 2016) and in sunflower, the modification of S metabolism has been suggested to be caused by a source effect (in particular serine availability), redox properties (oxidative situation at high photorespiration) and changes in metabolic effector concentration (such as *O*-acetylserine) (Abadie & Tcherkez, 2019b). Future studies are warranted to examine more closely rapid post-translational modifications of enzymes as well as absolute quantitation of metabolic effectors or hormones (such as ethylene) to provide more insight on mechanistic aspects.

ACKNOWLEDGMENT

The authors thank the technical support by the Joint Mass Spectrometry Facility at ANU and Dr. Adam Carroll for advices in LC–MS data alignment and extraction. The authors acknowledge the financial contribution of the Région Pays de la Loire and Angers Loire Métropole via the research grant Connect Talent Isoseed.

ORCID

Anis M. Limami https://orcid.org/0000-0002-9985-2363
Guillaume Tcherkez https://orcid.org/0000-0002-3339-956X

REFERENCES

Abadie, C., Bathellier, C., & Tcherkez, G. (2018). Carbon allocation to major metabolites in illuminated leaves is not just proportional to photosynthesis when gaseous conditions (CO_2 and O_2) vary. *New Phytologist*, *218*, 94–106.

Abadie, C., Blanchet, S., Carroll, A., & Tcherkez, G. (2017). Metabolomics analysis of post-photosynthetic effects of gaseous O_2 on primary metabolism in illuminated leaves. *Functional Plant Biology*, *44*, 929–940.

Abadie, C., Boex-Fontvieille, E. R., Carroll, A. J., & Tcherkez, G. (2016). In vivo stoichiometry of photorespiratory metabolism. *Nature Plants*, *2*, 1–4.

Abadie, C., Lothier, J., Boex-Fontvieille, E., Carroll, A. J., & Tcherkez, G. (2017). Direct assessment of the metabolic origin of carbon atoms in glutamate from illuminated leaves using ^{13}C-NMR. *New Phytologist*: In press, *216*, 1079–1089.

Abadie, C., Mainguet, S., Davanture, M., Hodges, M., Zivy, M., & Tcherkez, G. (2016). Concerted changes in the phosphoproteome and metabolome under different CO_2/O_2 gaseous conditions in *Arabidopsis* rosettes. *Plant and Cell Physiology*, *57*, 1544–1556.

Abadie, C., & Tcherkez, G. (2019a). In vivo phosphoenolpyruvate carboxylase activity is controlled by CO_2 and O_2 mole fractions and represents a major flux at high photorespiration rates. *New Phytologist*, *221*, 1843–1852.

Abadie, C., & Tcherkez, G. (2019b). Plant sulphur metabolism is stimulated by photorespiration. *Nature Communications Biology*, *2*, 1–7.

Atkin, O. K., Millar, A. H., Gardeström, P., & Day, D. A. (2000). Photosynthesis, carbohydrate metabolism and respiration in leaves of higher plants. In *Photosynthesis and respiration* (pp. 153–175). Amsterdam: Springer Netherlands.

Bloom, A., Burger, M., Kimball, B., & Pinter, P. (2014). Nitrate assimilation is inhibited by elevated CO_2 in field-grown wheat. *Nature Climate Change*, *4*, 477–480.

Bloom, A. J., Burger, M., Asensio, J. S. R., & Cousins, A. B. (2010). Carbon dioxide enrichment inhibits nitrate assimilation in wheat and *Arabidopsis*. *Science*, *328*, 899–903.

Boex-Fontvieille, E. R., Gauthier, P. P., Gilard, F., Hodges, M., & Tcherkez, G. (2013). A new anaplerotic respiratory pathway involving lysine biosynthesis in isocitrate dehydrogenase-deficient *Arabidopsis* mutants. *New Phytologist*, *199*, 673–682.

Busch, F. A. (2020). Photorespiration in the context of rubisco biochemistry, CO_2 diffusion and metabolism. *The Plant Journal*, *101*, 919–939.

Bykova, N. V., Keerberg, O., Pärnik, T., Bauwe, H., & Gardeström, P. (2005). Interaction between photorespiration and respiration in transgenic potato plants with antisense reduction in glycine decarboxylase. *Planta*, *222*, 130–140.

Bylesjö, M., Rantalainen, M., Cloarec, O., Nicholson, J. K., Holmes, E., & Trygg, J. (2006). OPLS discriminant analysis: Combining the strengths of PLS-DA and SIMCA classification. *Journal of Chemometrics: A Journal of the Chemometrics Society*, *20*, 341–351.

Carroll, A. J., Badger, M. R., & Millar, A. H. (2010). The MetabolomeExpress project: Enabling web-based processing, analysis and transparent dissemination of GC/MS metabolomics datasets. *BMC Bioinformatics*, *11*, 376.

Eriksson, L., Trygg, J., & Wold, S. (2008). CV-ANOVA for significance testing of PLS and OPLS® models. *Journal of Chemometrics: A Journal of the Chemometrics Society*, *22*, 594–600.

Gardeström, P., & Wigge, B. (1988). Influence of photorespiration on ATP/ADP ratios in the chloroplasts, mitochondria, and cytosol, studied by rapid fractionation of barley (*Hordeum vulgare*) protoplasts. *Plant Physiology*, *88*, 69–76.

Gauthier, P. P., Saenz, N., Griffin, K. L., Way, D., & Tcherkez, G. (2020). Is the Kok effect a respiratory phenomenon? Metabolic insight using ^{13}C labeling in *Helianthus annuus* leaves. *New Phytologist*: In press, *228*, 1243–1255.

Griffin, K., & Turnbull, M. (2013). Light saturated RuBP oxygenation by rubisco is a robust predictor of light inhibition of respiration in *Triticum aestivum* L. *Plant Biology*, *15*, 769–775.

Hanson, A. D., & Roje, S. (2001). One-carbon metabolism in higher plants. *Annual Review of Plant Biology*, *52*, 119–137.

Jacob, D., Deborde, C., Lefebvre, M., Maucourt, M., & Moing, A. (2017). NMRProcFlow: A graphical and interactive tool dedicated to 1D spectra processing for NMR-based metabolomics. *Metabolomics*, *13*, 36.

Maeda, H., & Dudareva, N. (2012). The shikimate pathway and aromatic amino acid biosynthesis in plants. *Annual Review of Plant Biology*, *63*, 73–105.

Mhamdi, A., Kerchev, P. I., Willems, P., Noctor, G., & Van Breusegem, F. (2017). Measurement of transcripts associated with photorespiration and related redox signaling. In A. Fernie, H. Bauwe, & A. Weber (Eds.), *Photorespiration* (pp. 17–29). New York, NY: Springer Humana Press.

Myers, O. D., Sumner, S. J., Li, S., Barnes, S., & Du, X. (2017). One step forward for reducing false positive and false negative compound identifications from mass spectrometry metabolomics data: New algorithms for constructing extracted ion chromatograms and detecting chromatographic peaks. *Analytical Chemistry*, *89*, 8696–8703.

Noctor, G., & Mhamdi, A. (2017). Climate change, CO_2, and defense: The metabolic, redox, and signaling perspectives. *Trends in Plant Science*, *22*, 857–870.

Pluskal, T., Korf, A., Smirnov, A., Schmid, R., Fallon, T. R., Du, X., & Weng, J.-K. (2020). Metabolomics data analysis using MZmine. In R. Winkler (Ed.), *Processing metabolomics and proteomics data with open software* (pp. 232–254). London: Royal Society of Chemistry.

Preiser, A. L., Fisher, N., Banerjee, A., & Sharkey, T. D. (2019). Plastidic glucose-6-phosphate dehydrogenases are regulated to maintain activity in the light. *Biochemical Journal*, *476*, 1539–1551.

Rachmilevitch, S., Cousins, A. B., & Bloom, A. J. (2004). Nitrate assimilation in plant shoots depends on photorespiration. *Proceedings of the National Academy of Sciences of the USA*, *101*, 11506–11510.

Sakihama, Y., Ji, M., Sano, S., Asada, K., & Yamasaki, H. (2000). Reduction of phenoxyl radicals mediated by monodehydroascorbate reductase. *Biochemical and Biophysical Research Communications*, *279*, 949–954.

Tcherkez, G., Bligny, R., Gout, E., Mahé, A., Hodges, M., & Cornic, G. (2008). Respiratory metabolism of illuminated leaves depends on CO_2 and O_2 conditions. *Proceedings of the National Academy of Sciences of the USA*, *105*, 797–802.

Tcherkez, G., Boex-Fontvieille, E., Mahé, A., & Hodges, M. (2012). Respiratory carbon fluxes in leaves. *Current Opinion in Plant Biology*, *15*, 308–314.

Tcherkez, G., Carroll, A., Abadie, C., Mainguet, S., Davanture, M., & Zivy, M. (2020). Protein synthesis increases with photosynthesis via the stimulation of translation initiation. *Plant Science*, *291*, 110352.

Tcherkez, G., Gauthier, P., Buckley, T. N., Busch, F. A., Barbour, M. M., Bruhn, D., … Cornic, G. (2017). Leaf day respiration: Low CO_2 flux but high significance for metabolism and carbon balance. *New Phytologist*, *216*, 986–1001.

Tcherkez, G., & Limami, A. M. (2019). Net photosynthetic CO_2 assimilation: More than just CO_2 and O_2 reduction cycles. *New Phytologist*, *223*, 520–529.

Tcherkez, G., Mahe, A., Guerard, F., Boex-Fontvieille, E. R. A., Gout, E., Lamothe, M., … Bligny, R. (2012). Short-term effects of CO_2 and O_2 on citrate metabolism in illuminated leaves. *Plant Cell and Environment*, *35*, 2208–2220.

von Caemmerer, S. (2013). Steady-state models of photosynthesis. *Plant Cell and Environment*, *36*, 1617–1630.

Yin, Z.-H., Dietz, K.-J., & Heber, U. (1990). Light-dependent pH changes in leaves of C_3 plants: III. Effect of inhibitors of photosynthesis and of the developmental state of the photosynthetic apparatus on cytosolic and vacuolar pH changes. *Planta*, *182*, 262–269.

Zrenner, R., Stitt, M., Sonnewald, U., & Boldt, R. (2006). Pyrimidine and purine biosynthesis and degradation in plants. *Annual Review of Plant Biology*, *57*, 805–836.

SUPPORTING INFORMATION

Additional supporting information may be found online in the Supporting Information section at the end of this article.

How to cite this article: Abadie C, Lalande J, Limami AM, Tcherkez G. Non-targeted ^{13}C metabolite analysis demonstrates broad re-orchestration of leaf metabolism when gas exchange conditions vary. *Plant Cell Environ*. 2020;1–13. https://doi.org/10.1111/pce.13940